Long-term Stabilized Amorphous Calcium Carbonate – an Ink for Bio-inspired 3D Printing

Hadar Shaked[a], Iryna Polishchuk [a], Alina Nagel [a], Yehonadav Bekenstein [a], and Boaz Pokroy*[a]

[a]Department of Materials Science and Engineering and the Russell Berrie Nanotechnology Institute, Technion – Israel Institute of Technology, 32000, Haifa, Israel.

Biominerals formed by organisms in the course of biomineralization often demonstrate complex morphologies despite their single-crystalline nature. This is achieved owing to the crystallization via a predeposited amorphous calcium carbonate (ACC) phase, a precursor that is particularly widespread in biominerals. Inspired by this natural strategy, we utilized robocasting, an additive manufacturing 3D-printing technique, for printing 3D objects from novel long-term, Mg-stabilized ACC pastes with high solids loading. We demonstrated, for the first time, that the ACC remains stable for at least a couple of months, even after printing. Crystallization, if desired, occurs only after the 3D object is already formed and at temperatures significantly lower than those of common post-printing sintering. We also examined the effects of different organic binders on the crystallization, the morphology, and the amount of incorporated Mg. This novel bio-inspired method may pave the way for a new bio-inspired route to low-temperature 3D printing of ceramic materials for a multitude of applications.

Introduction

Calcium carbonate ($CaCO_3$) is the biomineral most abundantly used by various organisms to form skeletons, protective shells, [1] teeth [2] and optical lenses.[3] While the commonest thermodynamically stable polymorphs of biogenic $CaCO_3$ are calcite and aragonite, the metastable polymorph amorphous calcium carbonate (ACC) has gained increasing interest owing to its widespread function as a precursor to crystalline $CaCO_3$. As a precursor, ACC leads to the formation of crystals exhibiting unique morphologies and enhanced physical properties.[2-9] Amorphous-to-crystalline transformation is known to facilitate the incorporation of organic and inorganic additives.[10-13] Mg is a common impurity in biogenic $CaCO_3$, and in biogenic calcite it can reach up to 40 at%,[14,15] a value substantially higher than its thermodynamic solubility limit (~2 at. %).[16] Incorporation of Mg is known to stabilize ACC, tune its hardness, change the morphology of the formed crystals and induce lattice distortions.[17-20] The ability to mimic the formation of intricately shaped crystals incorporating high amounts of various chemical species would be of great interest to materials scientists. Intracrystalline incorporation of additives is fragile and can be easily destroyed at high temperatures. [12,13] Our approach does not require processing at elevated temperatures thereby enabling the preservation of both the intricate shapes and the presence of even organic additives in the final crystalline lattice. Here, for the first time we demonstrate long-term stabilization of ACC thereafter used to form an easily handled ink and utilize it to form 3D models via an emerging technique of 3D printing. Bio-inspired 3D printing of ACC models may shed more light on the advantages of this phase from a materials point of view and deepen our understanding of the non-classical crystallization route commonly found in nature.

3D printing is a revolutionary manufacturing technique already used in various fields.[21-25] Given the growing demand for ceramic materials, several 3D printing methods have been developed for the fabrication of ceramic products.[26] Powder-based printing exploits the ability of a powder to bond in different mediums by using either laser sintering[27,28] or chemical binders.[29,30] Solids-based techniques employ solidified ceramic parts and reshape them to a final product by laser cutting, layering, and bonding[31] or by using binding powders to produce thermoplastic filaments.[32] Liquid-based techniques utilize photoreactive polymeric resins with embedded ceramic powders.[33,34] Robocasting is an additive manufacturing technique that is applicable in a wide variety of ceramic materials. Using this technique, a pre-prepared semi-liquid paste with high ceramic loading is extruded through a thin nozzle.[35,36] The paste is required to provide an appropriate viscosity under stress, allowing self-support and extrudability, and it should contain only a few, if any, agglomerates and a binder which, if required, can be easily removed after use.[37] The standard ceramic robocasting procedure forms a green body that usually requires high-temperature sintering. However, in our case, we eliminate the need in post-printing sintering, and enable low-temperature hardening of the printed material instead. Overcoming this limitation, will enable incorporation and preservation of various organic additives in a composite functional material which can be further employed in a variety of applications such as cultural heritage reconstruction, artificial reefs formation and bio-medical engineering (e.g., drug delivery).

Studies have revealed the potential inherent in bio-inspired 3D printing. Formation of highly porous ceramics inspired by wood and bones,[38,39] of hierarchical crack-controlled materials resembling nacre and spider silk,[40,41] and of superhydrophobic materials inspired by the lotus flower[42] are just a few examples. Bio-inspired 3D printing of crystalline calcium salts has focused mainly on calcium phosphates because of their abundance in natural organisms and their compatibility with bone-implant applications.[43-45] Currently, employment of calcium carbonate in 3D printing is mainly limited to crystalline powders bonded with aqueous binders.[46,47] Up to now, 3D printing of ACC has been contraindicated by its heat intolerance as well as by its inability to stabilize for long periods of time.

Here, by utilizing the robocasting method, we present an innovative route to the bio-inspired 3D printing of high Mg-ACC. We also introduce a novel storage protocol that allows to

maintain the amorphous nature of ACC powder for at least several days. In contrast to current technologies, our approach involves sintering at near-ambient temperatures and on-demand crystallization. We also examined the influence exerted by different organic binders on the crystalline structure and the morphology of the printed model.

Experimental

Powder preparation

Aqueous solutions of $CaCl_2 \cdot 2H_2O$ (73.5 g, 0.5 L), $MgCl_2 \cdot 6H_2O$ (101.655 g, 0.5 L) and Na_2CO_3 (52.995 g, 0.5 L) at 1 M concentration were prepared and stored overnight at 8°C. 50/50, 60/40 and 70/30 ratios of Ca:Mg solutions were mixed in a glass beaker for 5 min. An equivalent amount of Na_2CO_3 solution was added to the beaker with active mixing, preserving a 1:1 ion ratio between CO_3^{-2} and (Ca^{+2}+Mg^{+2}). The suspension was rapidly filtered through a Buchner funnel with grade 5 Whatman filter paper, followed by washing with water and acetone. After remaining under suction for 10 min, the filtered powder was dried for 3 h in a vacuum oven at 25 °C, 0.1 MPa. Storage of the dried ACC powder was maintained by its submergence in an excess of acetone.

Paste preparation

Stored powder was dried, ground with a mortar and pestle, and then mixed with dispersant (comprising corn oil at a fixed ratio of 0.1 ml per 1 g of powder) and varying amounts of 3 different binders. The powder was slowly added to the binder and hand mixed until a solid firm paste was obtained. Solids-loading of the mixed paste was kept between 52% and 65%, i.e. 1 g of powder for 0.5−0.8 ml of dispersant-binder mixture.

3D printing and post treatment

3D models were printed using the commercially available Hyrel 3D - Engine-SR printer with KR2-15 stainless steel extrusion head with a 1 mm nozzle. 3D-computer-aided design (3D-CAD) of the printed models was sketched using Fusion 360 (Autodesk). The 3D-CAD was converted to an .STL file, which was uploaded to the printer, where it was sliced, and the G-code was written. The printed models were placed in a vacuum oven for low-temperature sintering overnight at 150 °C, 0.1 MPa. The dry models were then transferred to the autoclave for the final crystallization step for 1 h at 100 °C, 0.1 MPa. Later, the models were dried in a vacuum oven for 3 h at 75 °C, 0.1 MPa.

High-Resolution Scanning Electron Microscopy

Samples were imaged using the Zeiss Ultra-Plus FEG-SEM at 1−2 kV. EDS was performed after carbon coating at 7 kV.

X-ray diffraction

Diffraction patterns of powdered samples were acquired using the Rikagu SmartLab 9 kW high-resolution diffraction system at a wavelength of Cu K-α 1.5406 Å and the Rigaku Miniflex benchtop powder XRD instrument at a wavelength of Cu K-α 1.5406 Å.

Rheology

Viscosity of the pastes was examined using the HR-2 Discovery Hybrid Rheometer, in rotational mode. Rheological measurements were performed at room temperature (25 °C) at constant shear of 10 s^{-1} with at least 3 replicates performed for each test. Approximately 1 cm^3 of paste was used in each experiment in a plate−plate geometry with 8 mm diameter. The gap between the plates was set to 1.3 mm.

Results and Discussion

Preparation of printable, stable Mg ACC paste and its viscosity

ACC was precipitated from solution in the presence of Mg. Different Ca:Mg ratios were tested, preserving a 1:1 ion ratio between $CO3^{-2}$ and (Ca^{+2}+Mg^{+2}). Each sample was labelled according to the Ca:Mg ratio used in the mixture, where 50/50 means 50% Ca solution and 50% Mg solution (e.g. 50 ml $CaCl_2$, 50 ml $MgCl_2$ and 100 ml $NaCO_3$ comprise 200 ml of sample solution), and the 60/40 and 70/30 solutions were labelled accordingly. Mixing of the solution resulted in the immediate precipitation of ACC. High amounts of ACC were synthesized from 1 M stock solutions, resulting in a yield of ~92%. To accumulate the amount of powder needed for 3D printing, an appropriate storage method was needed. We found that ACC powders, when stored in an excess of acetone, remain amorphous for long periods of time. This storage protocol enabled obtaining up to 40 gr of stabilized ACC in one experimental batch. As evidenced by X-ray Diffraction (XRD) patterns, the amorphous nature of ACC powder was preserved for 90-120 h after synthesis **(Fig 1A)** by its storage in an excess of acetone. Morphology of the synthesized ACC is depicted in **Fig 1B**. In order to prepare a printable paste, ACC powder was individually mixed with a dispersant (corn oil) and one of the 3 different binders — glycerol (GLY), ethylene glycol (EG) and triethylene glycol (TEG). Viscosities of the 50/50 resultant pastes were measured. Viscosity, among other parameters, is crucial in a printable paste that must be extrudable, non-phase-separating, durable and easily handled. The pastes prepared as described above undergo changes in viscosity over time. For a constant shear rate, a non-Newtonian shear-thinning behaviour was observed here, with viscosities ranging from 264,000 to 394,000 [cP], consistent with ceramic pastes with high solids loading. [48,49] No phase separation was observed in our pastes **(Fig 1C)**. Solids loading (i.e., the amount of suspended solids in a paste) has been shown to influence the final density of sintered ceramics.[50] High solids loadings are known to have a central role in the mechanical properties of the final product, resulting in a firmer and more stress-resilient ceramic part.[51,52] High solids-loading pastes (>65%) were difficult to measure as they cracked when applied with initial shear force; in addition, they were not easy to handle. In addition, lower solids loading pastes (<55%) could not be extruded without forcing phase separation. These findings led us to choose solids loadings of 55−65% in order to prevent undesirable results.

3D printing

3D printing of the prepared pastes was performed on aluminium foil, with the print bed wrapped for fast and easy transfer to the succeeding steps. The printing resolution was limited by the nozzle head used, which allowed accuracy within 1 mm. Initially, 2 “skirts” were printed around each model to allow priming of the extruder, thereby ensuring smooth and stable

flow. The ACC models were then printed and transferred to a vacuum oven for overnight sintering (150 °C, 0.1 MPa, 15 h), followed by exposure to humid conditions in autoclave (100 °C, 0.1 MPa, 1 h) for final crystallization. Following such treatment, printed models exhibited shape retention without dimensional distortions or significant cracks or fractures, and allowed removal of the binder by means of low-temperature sintering (**Fig 1D−F**). Owing to the limited thermal stability of ACC and its susceptibility to spinodal decomposition at ~400 °C,[12,13] sintering was done at a maximum temperature of 150 °C. This significant decrease in sintering temperatures is essential for energy conservation purposes.

Morphology and composition

Changes in morphology, depending on the binder used, were observed. In EG- and TEG-printed models the spherical morphology of ACC was preserved after the sintering step (**Fig 2 D−I**). On the other hand, the crystalline morphologies of GLY 60/40 and 70/30 models revealed clear rhombohedral facets (**Fig 2 B-C**), implying that crystallization had probably occurred during the sintering step. We believe that a "feeding-stock" phenomenon takes place, leading to the possibility of slow-paced crystallization in which the ACC particles are used as a calcium carbonate reservoir, as observed in biomineralization in nature (**Fig 2 B, C insets**).[53,54] After autoclave treatment the morphology changed drastically, and crystalline morphology can be seen in all models (**Fig S1)**.

Chemical compositions of the sintered ACC models and their respective Ca:Mg ratios were analysed by means of energy-dispersive spectroscopy (EDS) (**Fig S2**). As expected, the 50/50 ACC models exhibited higher levels of Mg incorporation than the 60/40 or 70/30 models. The highest level of incorporated Mg, with ~36 at%, was observed in the case of the 50/50 GLY model, and the higher the Mg content, the more significant the difference in incorporation between GLY and the other binders. We assume that stabilization of ACC obtained with TEG and EG binders may result in faster diffusion routes for Mg ions, while the GLY binder boosts crystallization, altogether leading to more complicated diffusion routes that result in higher levels of Mg incorporation.

Crystallization of the ACC models

The relationship between the binder and the crystallization process was examined in both the oven sintering and the autoclave crystallization post-printing steps. After oven sintering, both the EG- and the TEG-stabilized ACC models preserved their amorphous nature, showing a very mild degree of crystallization. The 70/30 models showed susceptibility to crystallization owing to their reduced stability associated with their lower levels of Mg incorporation (**Fig 3A−C**). The smallest amount of crystallization after oven sintering was that of calcite with its clear (006) preferred orientation, as well as of some aragonite revealing the (221) and (123) diffraction peaks (**Fig S3**). On the other hand, the GLY-stabilized ACC model demonstrated complete crystallization after oven sintering, which can be attributed to its highly hygroscopic nature[55]. The high-humidity environment within the autoclave facilitated rapid crystallization of all models, resulting in the formation of both calcite and aragonite phases. (**Fig 3D−F**). Further evidence of Mg incorporation into the structure of the printed models upon amorphous-to-crystalline transformation is provided by the shift in the (104) diffraction peak position to higher 2θ angles (smaller ion than that of Ca).[55,56]

Profile fitting[57] of the (104) single-diffraction peak revealed a relationship between the binder and the crystallite size (**Fig S4**). GLY was able to promote the formation of larger crystals than those formed with EG; the smallest crystals were observed when TEG was used as binder. This trend was observed for all samples with varying Ca:Mg ratios, confirming a clear dependency between grain size and binder. GLY was the only binder that promoted slow crystallization during the oven treatment,

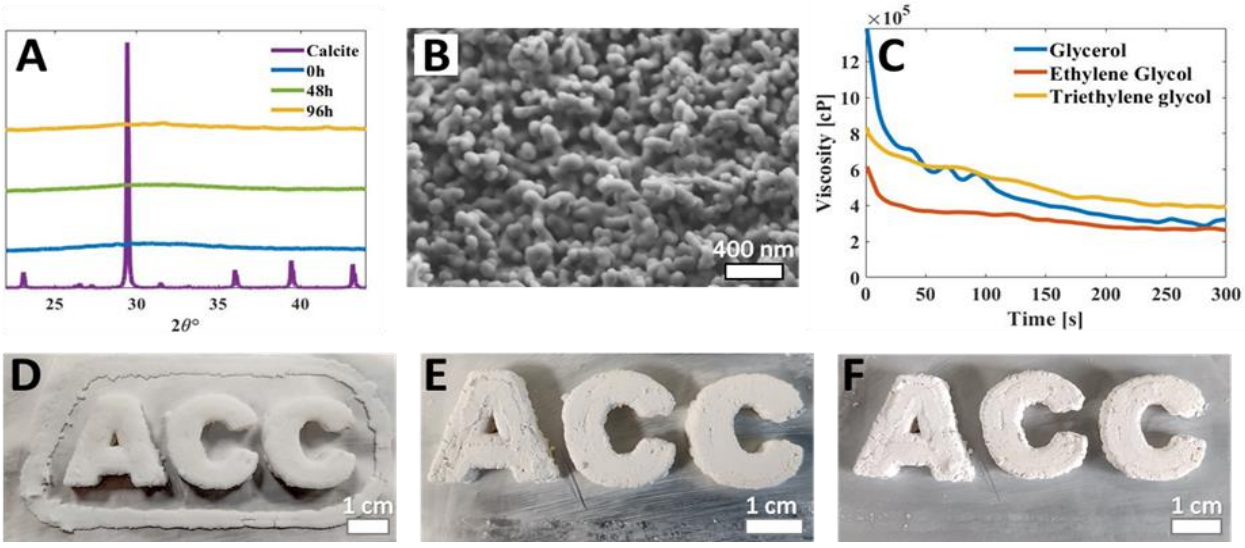

Fig. 1 (A) XRD patterns collected at a wavelength of Cu K-α 1.5406 Å from "as synthesized" (0 h) powdered ACC following its storage in acetone excess for 48 and 96 h. Diffraction patterns are compared with that of crystalline calcite. (B) High-resolution scanning electron microscope (HR-SEM) image demonstrating the morphology of obtained ACC. (C) Viscosity of prepared 50/50 pastes as a function of time for a constant shear rate. The decrease in viscosity over time until a plateau is reached is consistent with non-Newtonian shear thinning materials.[49] (D–F) ACC printed models from EG paste forming the word "ACC", (D) immediately after printing, (E) after low-temperature sintering, and (F) after crystallization treatment in an autoclave. Sample height, 6 mm.

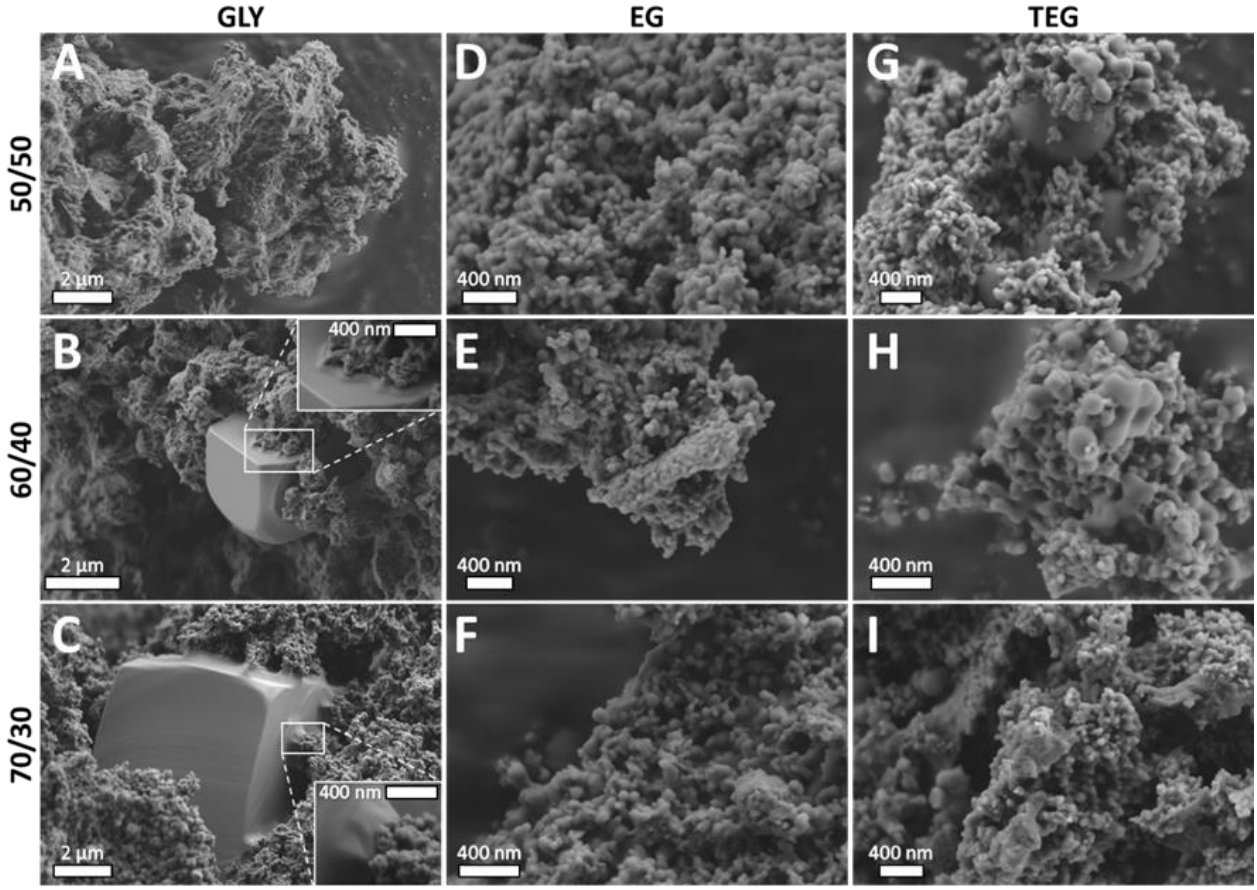

Fig. 2 - HR-SEM images of the 3D-printed models after sintering. A–C, with GLY binder; D–F, with EG binder; G–I, with TEG binder. Insets in B and C show magnified images of the "feeding-stock" phenomenon.

whereas in the presence of either EG or TEG, crystallization was rapidly induced by the humid environment within the autoclave. Therefore, slower growth rates led to the formation of larger crystals, while rapid crystallization promoted the formation of smaller crystals.

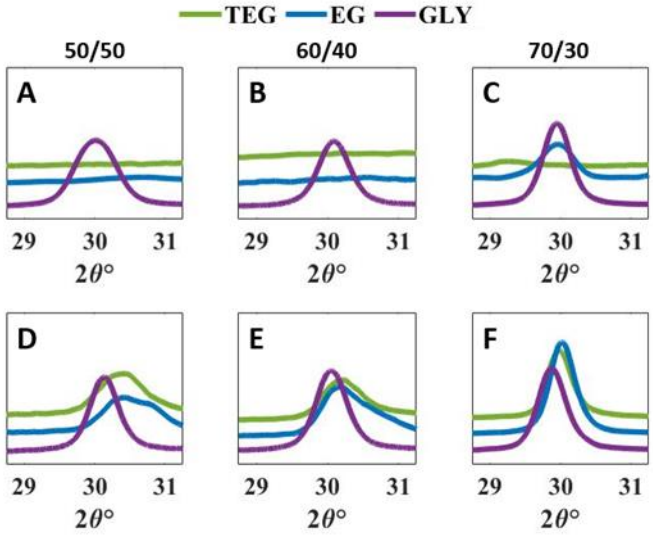

Fig 3 - The (104) diffraction peak of calcite (XRD patterns collected at wavelength Cu K-α 1.5406 Å). A–C, after oven treatment; B–F, after autoclave treatment.

Conclusions

This study presents a novel bio-inspired approach to the printing of 3D complex structures utilizing robocasting of printable, long-term stabilized ACC pastes with high solids loading (55−65%). Stabilization of ACC was achieved by the incorporation of foreign atoms such as Mg as well as by the storage environment. The amorphous nature of the obtained printable ACC pastes was retained for up to some months, even after low-temperature sintering at 150 °C. The post-sintered printed ACC 3D models exhibited no shrinkage and maintained their initial dimensions and complex shapes. We further showed that the choice of binder affected the amount of incorporated Mg, as well as the stabilization and the final morphology of the ACC models. EG and TEG preserved the amorphous nature of the ACC models for up to several months after printing, whereas GLY boosted their crystallization. GLY also facilitated the formation of larger crystals with higher Mg incorporation. In addition, GLY presented a "feeding-stock" morphology resembling that of ACC transformation to a crystalline phase in nature, thereby serving as a $CaCO_3$ reservoir enabling the formation of large crystals with unique morphologies and enhanced characteristics. This novel approach to 3D printing of ACC may highlight the advantages of this phase as a precursor to crystalline $CaCO_3$ and open new routes to energy-efficient 3D printing of ceramics for multiple applications.

Conflict of interests

There are no conflicts to declare.

Acknowledgments

This research was partly funded by the European Research Council under the European Union's Seventh Framework Program (FP/2013-2018)/ERC Grant Agreement no. 336077

References

(1) Aizenberg, J.; Weiner, S.; Addadi, L. Coexistence of Amorphous and Crystalline Calcium Carbonate in Skeletal Tissues. Connective Tissue Research 2003, 44 (1), 20–25. https://doi.org/10.1080/03008200390152034.

(2) Beniash, E.; Aizenberg, J.; Addadi, L.; Weiner, S. Amorphous Calcium Carbonate Transforms into Calcite during Sea Urchin Larval Spicule Growth. Proceedings of the Royal Society of London. Series B: Biological Sciences 1997, 264 (1380), 461–465. https://doi.org/10.1098/rspb.1997.0066.

(3) Aizenberg, J.; Tkachenko, A.; Weiner, S.; Addadi, L.; Hendler, G. Calcitic Microlenses as Part of the Photoreceptor System in Brittlestars. Nature 2001, 412 (6849), 819–822. https://doi.org/10.1038/35090573.

(4) Weiner, S.; Addadi, L. Crystallization Pathways in Biomineralization. Annual Review of Materials Research 2011, 41 (1), 21–40. https://doi.org/10.1146/annurev-matsci-062910-095803.

(5) Addadi, L.; Raz, S.; Weiner, S. Taking Advantage of Disorder: Amorphous Calcium Carbonate and Its Roles in Biomineralization. Advanced Materials 2003, 15 (12), 959–970. https://doi.org/10.1002/adma.200300381.

(6) Xu, A.-W.; Ma, Y.; Cölfen, H. Biomimetic Mineralization. J. Mater. Chem. 2007, 17 (5), 415–449. https://doi.org/10.1039/B611918M.

(7) Olszta, M. J.; Odom, D. J.; Douglas, E. P.; Gower, L. B. A New Paradigm for Biomineral Formation: Mineralization via an Amorphous Liquid-Phase Precursor. Connective Tissue Research 2003, 44 (1), 326–334. https://doi.org/10.1080/03008200390181852.

(8) Nassif, N.; Pinna, N.; Gehrke, N.; Antonietti, M.; Jager, C.; Colfen, H. Amorphous Layer around Aragonite Platelets in Nacre. Proceedings of the National Academy of Sciences 2005, 102 (36), 12653–12655. https://doi.org/10.1073/pnas.0502577102.

(9) Gower, L. B.; Odom, D. J. Deposition of Calcium Carbonate Films by a Polymer-Induced Liquid-Precursor (PILP) Process. Journal of Crystal Growth 2000, 210 (4), 719–734. https://doi.org/10.1016/S0022-0248(99)00749-6.

(10) Borukhin, S.; Bloch, L.; Radlauer, T.; Hill, A. H.; Fitch, A. N.; Pokroy, B. Screening the Incorporation of Amino Acids into an Inorganic Crystalline Host: The Case of Calcite. Advanced Functional Materials 2012, 22 (20), 4216–4224. https://doi.org/10.1002/adfm.201201079.

(11) Kim, Y.-Y.; Carloni, J. D.; Demarchi, B.; Sparks, D.; Reid, D. G.; Kunitake, M. E.; Tang, C. C.; Duer, M. J.; Freeman, C. L.; Pokroy, B.; Penkman, K.; Harding, J. H.; Estroff, L. A.; Baker, S. P.; Meldrum, F. C. Tuning Hardness in Calcite by Incorporation of Amino Acids. Nature Materials 2016, 15 (8), 903–910. https://doi.org/10.1038/nmat4631.

(12) Polishchuk, I.; Bracha, A. A.; Bloch, L.; Levy, D.; Kozachkevich, S.; Etinger-Geller, Y.; Kauffmann, Y.; Burghammer, M.; Giacobbe, C.; Villanova, J.; Hendler, G.; Sun, C. Y.; Giuffre, A. J.; Marcus, M. A.; Kundanati, L.; Zaslansky, P.; Pugno, N. M.; Gilbert, P. U. P. A.; Katsman, A.; Pokroy, B. Coherently Aligned Nanoparticles within a Biogenic Single Crystal: A Biological Prestressing Strategy. Science 2017, 358 (6368), 1294–1298. https://doi.org/10.1126/science.aaj2156.

(13) Seknazi, E.; Kozachkevich, S.; Polishchuk, I.; Bianco Stein, N.; Villanova, J.; Suuronen, J. P.; Dejoie, C.; Zaslansky, P.; Katsman, A.; Pokroy, B. From Spinodal Decomposition to Alternating Layered Structure within Single Crystals of Biogenic Magnesium Calcite. Nature Communications 2019, 10 (1), 1–9. https://doi.org/10.1038/s41467-019-12168-8.

(14) Raz, S.; Weiner, S.; Addadi, L. Formation of High-Magnesian Calcites via an Amorphous Precursor Phase: Possible Biological Implications. Advanced Materials 2000, 12 (1), 38–42. https://doi.org/10.1002/(SICI)1521-4095(200001)12:1<38::AID-ADMA38>3.0.CO;2-I.

(15) Falini, G.; Gazzano, M.; Ripamonti, A. Crystallization of Calcium Carbonate in Presence of Magnesium and Polyelectrolytes. Journal of Crystal Growth 1994, 137 (3–4), 577–584. https://doi.org/10.1016/0022-0248(94)91001-4.

(16) Politi, Y.; Batchelor, D. R.; Zaslansky, P.; Chmelka, B. F.; Weaver, J. C.; Sagi, I.; Weiner, S.; Addadi, L. Role of Magnesium Ion in the Stabilization of Biogenic Amorphous Calcium Carbonate: A Structure−Function Investigation. Chemistry of Materials 2010, 22 (1), 161–166. https://doi.org/10.1021/cm902674h.

(17) Ma, Y.; Cohen, S. R.; Addadi, L.; Weiner, S. Sea Urchin Tooth Design: An "All-Calcite" Polycrystalline Reinforced Fiber Composite for Grinding Rocks. Advanced Materials 2008, 20 (8), 1555–1559. https://doi.org/10.1002/adma.200702842.

(18) Rodriguez-Blanco, J. D.; Shaw, S.; Bots, P.; Roncal-Herrero, T.; Benning, L. G. The Role of PH and Mg on the Stability and Crystallization of Amorphous Calcium Carbonate. Journal of Alloys and Compounds 2012, 536, S477–S479. https://doi.org/10.1016/j.jallcom.2011.11.057.

(19) Loste, E.; Wilson, R. M.; Seshadri, R.; Meldrum, F. C. The Role of Magnesium in Stabilising Amorphous Calcium Carbonate and Controlling Calcite Morphologies. Journal of Crystal Growth 2003, 254 (1–2), 206–218. https://doi.org/10.1016/S0022-0248(03)01153-9.

(20) Seknazi, E.; Pokroy, B. Residual Strain and Stress in Biocrystals. Advanced Materials 2018, 30 (41), 1–6. https://doi.org/10.1002/adma.201707263.

(21) Compton, B. G.; Lewis, J. A. 3D-Printing of Lightweight Cellular Composites. Advanced Materials 2014, 26 (34), 5930–5935. https://doi.org/10.1002/adma.201401804.

(22) Sun, K.; Wei, T.-S.; Ahn, B. Y.; Seo, J. Y.; Dillon, S. J.; Lewis, J. A. 3D Printing of Interdigitated Li-Ion Microbattery Architectures. Advanced Materials 2013, 25 (33), 4539–4543. https://doi.org/10.1002/adma.201301036.

(23) Kolesky, D. B.; Truby, R. L.; Gladman, A. S.; Busbee, T. A.; Homan, K. A.; Lewis, J. A. 3D Bioprinting of Vascularized, Heterogeneous Cell-Laden Tissue Constructs. Advanced Materials 2014, 26 (19), 3124–3130. https://doi.org/10.1002/adma.201305506.

(24) Kamyshny, A.; Magdassi, S. Conductive Nanomaterials for Printed Electronics. Small 2014, 10 (17), 3515–3535. https://doi.org/10.1002/smll.201303000.

(25) Zhou, N.; Bekenstein, Y.; Eisler, C. N.; Zhang, D.; Schwartzberg, A. M.; Yang, P.; Alivisatos, A. P.; Lewis, J. A. Perovskite Nanowire–Block Copolymer Composites with Digitally Programmable Polarization Anisotropy. Science Advances 2019, 5 (5), eaav8141. https://doi.org/10.1126/sciadv.aav8141.

(26) Chen, Z.; Li, Z.; Li, J.; Liu, C.; Lao, C.; Fu, Y.; Liu, C.; Li, Y.; Wang, P.; He, Y. 3D Printing of Ceramics: A Review. Journal of the European Ceramic Society 2019, 39 (4), 661–687. https://doi.org/10.1016/j.jeurceramsoc.2018.11.013.

(27) Bertrand, P.; Bayle, F.; Combe, C.; Goeuriot, P.; Smurov, I. Ceramic Components Manufacturing by Selective Laser Sintering. Applied Surface Science 2007, 254 (4), 989–992. https://doi.org/10.1016/j.apsusc.2007.08.085.

(28) Deckers, J.; Meyers, S.; Kruth, J. P.; Vleugels, J. Direct Selective Laser Sintering/Melting of High Density Alumina Powder Layers at Elevated Temperatures. Physics Procedia 2014, 56 (C), 117–124. https://doi.org/10.1016/j.phpro.2014.08.154.

(29) Will, J.; Melcher, R.; Treul, C.; Travitzky, N.; Kneser, U.; Polykandriotis, E.; Horch, R.; Greil, P. Porous Ceramic Bone Scaffolds for Vascularized Bone Tissue Regeneration. Journal of Materials Science: Materials in Medicine 2008, 19 (8), 2781–2790. https://doi.org/10.1007/s10856-007-3346-5.

(30) Ke, D.; Bose, S. Effects of Pore Distribution and Chemistry on Physical, Mechanical, and Biological Properties of Tricalcium Phosphate Scaffolds by Binder-Jet 3D Printing. Additive Manufacturing 2018, 22 (July 2017), 111–117. https://doi.org/10.1016/j.addma.2018.04.020.

(31) Dermeik, B.; Travitzky, N. Laminated Object Manufacturing of Ceramic-Based Materials. Advanced Engineering Materials 2020, 22 (9), 2000256. https://doi.org/10.1002/adem.202000256.

(32) Sa, M.; Nguyen, B. B.; Moriarty, R. A.; Kamalitdinov, T.; Fisher, J. P.; Kim, J. Y. Fabrication and Evaluation of 3D Printed BCP Scaffolds Reinforced with ZrO 2 for Bone Tissue Applications. Biotechnology and Bioengineering 2018, 115 (4), 989–999. https://doi.org/10.1002/bit.26514.

(33) Shukrun Farrell, E.; Schilt, Y.; Moshkovitz, M. Y.; Levi-Kalisman, Y.; Raviv, U.; Magdassi, S. 3D Printing of Ordered Mesoporous Silica Complex Structures. Nano Letters 2020, 20 (9), 6598–6605. https://doi.org/10.1021/acs.nanolett.0c02364.

(34) Cooperstein, I.; Indukuri, S. R. K. C.; Bouketov, A.; Levy, U.; Magdassi, S. 3D Printing of Micrometer-Sized Transparent Ceramics with On-Demand Optical-Gain Properties. Advanced Materials 2020, 32 (28), 2001675. https://doi.org/10.1002/adma.202001675.

(35) Peng, E.; Zhang, D.; Ding, J. Ceramic Robocasting: Recent Achievements, Potential, and Future Developments. Advanced Materials 2018, 30 (47), 1802404. https://doi.org/10.1002/adma.201802404.

(36) Zocca, A.; Colombo, P.; Gomes, C. M.; Günster, J. Additive Manufacturing of Ceramics: Issues, Potentialities, and Opportunities. Journal

of the American Ceramic Society 2015, 98 (7), 1983–2001. https://doi.org/10.1111/jace.13700.

(37) Travitzky, N.; Bonet, A.; Dermeik, B.; Fey, T.; Filbert-Demut, I.; Schlier, L.; Schlordt, T.; Greil, P. Additive Manufacturing of Ceramic-Based Materials. Advanced Engineering Materials 2014, 16 (6), 729–754. https://doi.org/10.1002/adem.201400097.

(38) Minas, C.; Carnelli, D.; Tervoort, E.; Studart, A. R. 3D Printing of Emulsions and Foams into Hierarchical Porous Ceramics. Advanced Materials 2016, 28 (45), 9993–9999. https://doi.org/10.1002/adma.201603390.

(39) Alison, L.; Menasce, S.; Bouville, F.; Tervoort, E.; Mattich, I.; Ofner, A.; Studart, A. R. 3D Printing of Sacrificial Templates into Hierarchical Porous Materials. Scientific Reports 2019, 9 (1), 409. https://doi.org/10.1038/s41598-018-36789-z.

(40) X. Gu, G.; Su, I.; Sharma, S.; Voros, J. L.; Qin, Z.; Buehler, M. J. Three-Dimensional-Printing of Bio-Inspired Composites. Journal of Biomechanical Engineering 2016, 138 (2), 1–16. https://doi.org/10.1115/1.4032423.

(41) Mirzaeifar, R.; Dimas, L. S.; Qin, Z.; Buehler, M. J. Defect-Tolerant Bioinspired Hierarchical Composites: Simulation and Experiment. ACS Biomaterials Science & Engineering 2015, 1 (5), 295–304. https://doi.org/10.1021/ab500120f.

(42) Xing, R.; Huang, R.; Qi, W.; Su, R.; He, Z. Three-Dimensionally Printed Bioinspired Superhydrophobic PLA Membrane for Oil-Water Separation. AIChE Journal 2018, 64 (10), 3700–3708. https://doi.org/10.1002/aic.16347.

(43) Bergmann, C.; Lindner, M.; Zhang, W.; Koczur, K.; Kirsten, A.; Telle, R.; Fischer, H. 3D Printing of Bone Substitute Implants Using Calcium Phosphate and Bioactive Glasses. Journal of the European Ceramic Society 2010, 30 (12), 2563–2567. https://doi.org/10.1016/j.jeurceramsoc.2010.04.037.

(44) Miranda, P.; Saiz, E.; Gryn, K.; Tomsia, A. P. Sintering and Robocasting of β-Tricalcium Phosphate Scaffolds for Orthopaedic Applications. Acta Biomaterialia 2006, 2 (4), 457–466. https://doi.org/10.1016/j.actbio.2006.02.004.

(45) Trombetta, R.; Inzana, J. A.; Schwarz, E. M.; Kates, S. L.; Awad, H. A. 3D Printing of Calcium Phosphate Ceramics for Bone Tissue Engineering and Drug Delivery. Annals of Biomedical Engineering 2017, 45 (1), 23–44. https://doi.org/10.1007/s10439-016-1678-3.

(46) Mohan, D.; Khairullah, N. F.; How, Y. P.; Sajab, M. S.; Kaco, H. 3D Printed Laminated CaCO3-Nanocellulose Films as Controlled-Release 5-Fluorouracil. Polymers 2020, 12 (4), 986. https://doi.org/10.3390/polym12040986.

(47) Leu, M. C.; Deuser, B. K.; Landers, R. G.; Hilmas, G. E.; Watts, J. L. Freeze-Form Extrusion Fabrication of Functionally Graded Materials. CIRP Annals - Manufacturing Technology 2012, 61. https://doi.org/10.1016/j.cirp.2012.03.050.

(48) Zima, A.; Czechowska, J.; Siek, D.; Ślósarczyk, A. Influence of Magnesium and Silver Ions on Rheological Properties of Hydroxyapatite/Chitosan/Calcium Sulphate Based Bone Cements. Ceramics International 2017, 43 (18), 16196–16203. https://doi.org/10.1016/j.ceramint.2017.08.197.

(49) Ryabenkova, Y.; Pinnock, A.; Quadros, P. A.; Goodchild, R. L.; Möbus, G.; Crawford, A.; Hatton, P. V.; Miller, C. A. The Relationship between Particle Morphology and Rheological Properties in Injectable Nano-Hydroxyapatite Bone Graft Substitutes. Materials Science and Engineering: C 2017, 75, 1083–1090. https://doi.org/10.1016/j.msec.2017.02.170.

(50) Ferreira, J. M. F.; Diz, H. M. M. Effect of Solids Loading on Slip-Casting Performance of Silicon Carbide Slurries. Journal of the American Ceramic Society 1999, 82 (8), 1993–2000. https://doi.org/10.1111/j.1151-2916.1999.tb02031.x.

(51) Wei, J.; Li, J.; Song, X.; Feng, Y.; Qiu, T. Effects of Solid Loading on the Rheological Behaviors and Mechanical Properties of Injection-Molded Alumina Ceramics. Journal of Alloys and Compounds 2018, 768, 503–509. https://doi.org/10.1016/j.jallcom.2018.07.036.

(52) Chen, T.; Sun, A.; Chu, C.; Wu, H.; Wang, J.; Wang, J.; Li, Z.; Guo, J.; Xu, G. Rheological Behavior of Titania Ink and Mechanical Properties of Titania Ceramic Structures by 3D Direct Ink Writing Using High Solid Loading Titania Ceramic Ink. Journal of Alloys and Compounds 2019, 783, 321–328. https://doi.org/10.1016/j.jallcom.2018.12.334.

(53) Han, T. Y.-J.; Aizenberg, J. Calcium Carbonate Storage in Amorphous Form and Its Template-Induced Crystallization †. Chemistry of Materials 2008, 20 (3), 1064–1068. https://doi.org/10.1021/cm702032v.

(54) Raz, S.; Testeniere, O.; Hecker, A.; Weiner, S.; Luquet, G. Stable Amorphous Calcium Carbonate Is the Main Component of the Calcium Storage Structures of the Crustacean Orchestia Cavimana. The Biological Bulletin 2002, 203 (3), 269–274. https://doi.org/10.2307/1543569.

(55) Alber, H. K. Hygroscopic Substances in Microanalysis. Mikrochemie 1938, 25 (1), 167–181. https://doi.org/10.1007/BF02714760.

(56) Bianco-Stein, N.; Polishchuk, I.; Seiden, G.; Villanova, J.; Rack, A.; Zaslansky, P.; Pokroy, B. Helical Microstructures of the Mineralized Coralline Red Algae Determine Their Mechanical Properties. Advanced Science 2020, 7 (11), 2000108. https://doi.org/10.1002/advs.202000108.

(57) Pokroy, B.; Fitch, A.; Zolotoyabko, E. The Microstructure of Biogenic Calcite: A View by High-Resolution Synchrotron Powder Diffraction. Advanced Materials 2006, 18 (18), 2363–2368. https://doi.org/10.1002/adma.200600714.